T. Bierkandt, P. Hemberger, P. Oßwald, M. Köhler, T. Kasper, Insights in m-xylene decomposition under fuel-rich conditions by imaging photoelectron photoion coincidence spectroscopy, Proc. Combust. Inst. 36 (2017) 1223-1232.

[doi 10.1016/j.proci.2016.06.143]

Insights in *m*-xylene decomposition under fuel-rich conditions by imaging photoelectron photoion coincidence spectroscopy

Thomas Bierkandt[1], Patrick Hemberger[2], Patrick Oßwald[3], Markus Köhler[3], Tina Kasper[1*]

[1]Mass Spectrometry in Reactive Flows – Thermodynamics, IVG, University of Duisburg-Essen, D-47057 Duisburg, Germany

[2]Molecular Dynamics Group, Paul Scherrer Institute, 5232 Villigen PSI, Switzerland

[3]Institute of Combustion Technology, German Aerospace Center (DLR), Pfaffenwaldring 38-40, D-70569 Stuttgart, Germany

*Corresponding Author: Tina Kasper, Thermodynamics, Lotharstr. 1, 47057 Duisburg, Germany
phone: +49-203-379-1854, fax: +49-203-379-1250
email: tina.kasper@uni-due.de

Colloquium Topic Area: **Laminar Flames,**
Reaction Kinetics (alternative session)

Word counts (method 1)

Part	Method	# words
Abstract	Microsoft Word 2010 word count	300
Main text	Microsoft Word 2010 word count	3497
Equations	(0) lines × 7.6 words/line	0
References	(41 + 2) × 2.3 lines/ref × 7.6 words/line	751
Tables	[(0+2)*1 + (+2)*1 + (+2)] × 7.6 words/line	0
Figure 1	[(49.8 mm + 10 mm) × 2.2 words/mm × 1] + 32	163
Figure 2	[(116.7 mm + 10 mm) × 2.2 words/mm × 2] + 14	571
Figure 3	[(58.0 mm + 10 mm) × 2.2 words/mm × 1] + 33	182
Figure 4	[(57.0 mm + 10 mm) × 2.2 words/mm × 1] + 19	166
Figure 5	[(58.0 mm + 10 mm) × 2.2 words/mm × 1] + 39	188
Figure 6	[(73.1 mm + 10 mm) × 2.2 words/mm × 1] + 7	189
Figure 7	[(58.7 mm + 10 mm) × 2.2 words/mm × 1] + 19	170
Figure 8	[(53.1 mm + 10 mm) × 2.2 words/mm × 1] + 10	148
Figure 9	[(57.3 mm + 10 mm) × 2.2 words/mm × 1] + 16	164
Total (excl. abstract)		**6189**

Supplemental material has been included in the submission of this paper.

Submitted to the 36th International Symposium on Combustion, Seoul, 2016

Color figures in electronic version only.

Abstract

A fuel-rich (Φ=1.79) *m*-xylene flame (7.3% *m*-C_8H_{10}, 42.7% O_2, 50.0% Ar) at low-pressure (40 mbar) was investigated with focus on the reactive fuel radicals (C_8H_9) and the first decomposition steps leading to C_8H_8 isomers. The results show that an isomerization of the *m*-xylyl radical to *o*- and *p*-xylyl must take place to explain the observed intermediates in agreement with pyrolysis experiments. Important higher polycyclic aromatic hydrocarbons (PAHs) relevant to soot formation were also identified. All Measurements were performed with a molecular-beam mass spectrometry (MBMS) setup at the Swiss Light Source (SLS), where single-photon ionization with VUV radiation offers soft ionization of the sampled species. Isomer-selective detection with unprecedented resolution is achieved by a combination of time-of-flight mass spectrometry and imaging photoelectron photoion coincidence (iPEPICO) spectroscopy. In principle, species can be identified by comparison of measured ionization efficiency (PIE) curves with known or calculated ionization energies of expected species. For convoluted signals of several species this procedure works well for the isomer with the lowest ionization energy. Changes in the slopes of the ionization efficiency curve do not necessarily correlate with ionization thresholds of other isomers and the assignment of higher thresholds can become difficult. PEPICO spectrometry, which detects the electrons that are produced in the ionization process in coincidence with the ions, enables the measurement of mass-selected threshold photoelectron spectra (ms-TPES). These spectra improve the detection capability of isomers because vibrational transitions from the neutral into ionic states can be observed and used as a fingerprint of a specific molecule. The obtained ms-TPES are compared with reference spectra from the literature or Franck-Condon simulations. Quantification of the major species as well as several intermediate species for this fuel-rich *m*-xylene flame yields a data set for model validation and experimental results are compared with five kinetic reaction models from the literature.

Keywords: *m*-xylene flame structure, laminar premixed flame, molecular-beam mass spectrometry, VUV photoionization, soot precursors

1. Introduction

Although the amount of alternative energy carriers is increasing, currently 80% of the world energy consumption is covered by fossil fuels and they will remain the most important primary energy carrier in coming years [1]. Especially, the global demand for liquid fuels for transportation produced from crude oil is still rising due to increasing population and economic growth [2] and is associated with harmful emissions of polyaromatic hydrocarbons (PAHs), soot, oxygenates, NO_x, and volatile organic compounds (VOCs). To control the emissions a more detailed understanding of the combustion processes is still necessary. Especially, the investigation of reactive combustion intermediates is crucial because they influence pollutant formation. The monoaromatic hydrocarbons benzene, toluene, ethylbenzene, and the three xylene isomers belong to the VOCs and can be found with up to 20% (w/w) in typical gasoline blends [3]. Xylenes are the simplest dialkyl-substituted aromatic compounds and they are differentiated by the position of the methyl groups as *ortho*- (1,2-dimethylbenzene), *meta*- (1,3-dimethylbenzene), and *para*-xylene (1,4-dimethylbenzene). Xylenes accounts for the highest fraction and can improve the antiknock properties of the gasoline [4]. The use of biodiesel and ethanol as surrogate to Diesel fuel can help to decrease the overall concentrations of monoaromatic hydrocarbons in the exhaust gas of combustion engines, as shown by Di et al. [5], but the concentration of oxygenates is increased. Because xylenes are present in gasoline several investigations of their combustion and oxidation behavior under different conditions have been performed, previously.

Investigations in shock tubes [6, 7] find that *o*-xylene is the most reactive isomer. Ignition delay times and species profiles were measured for *m*-xylene under lean, stoichiometric, and fuel-rich conditions in a single-pulse shock tube by Gudiyella et al. [8]. The oxidation of *p*-xylene and *m*-xylene was investigated in a jet-stirred reactor at atmospheric pressure [9, 10]. Laminar burning

velocities of benzene and some alkylbenzenes including *m*-xylene were measured in a combustion vessel at 3 bar and 450 K for different equivalence ratios by Johnston and Farrell [11]. They found that burning velocities depend on the length and the number of alkylated side chains with benzene as the fastest and *m*-xylene as the slowest of the observed compounds. Similar observations are reported for the laminar flame speeds measured in the counterflow configuration at atmospheric pressure with benzene as the fastest [12]. Differences between the xylene isomers are small under lean conditions (slightly faster flame speed for *o*-xylene) and disappear under fuel-rich conditions. Mouis et al. [13] investigated the effect of *m*-xylene on soot in laminar ethylene co-flow diffusion flames from 1 to 5 atm. The pyrolysis of the xylyl radicals, as the first decomposition product of xylenes in combustion processes, was studied in detail experimentally by iPEPICO from the pyrolysis of xylyl bromides in a SiC reactor by Hemberger et al. [14, 15] and theoretically in [16, 17].

While there are a number of studies on the combustion and oxidation of xylenes at atmospheric or higher pressure there are few studies on laminar low-pressure flames [3, 4, 9]. The work of Li et al. [3] reports the identification of combustion intermediates up to a *m/z* ratio of 240 in fuel-rich monocyclic aromatic hydrocarbons including xylene isomers at 40 mbar by MBMS. By comparison of signal intensities of different PAHs they concluded that xylenes have the highest sooting tendency of the investigated fuels. Also the results of [18] support that m-xylene has a relatively high sooting tendency in comparison to other aromatic hydrocarbons like benzene or toluene. A detailed measurement of species mole fraction profiles in laminar premixed *o*-xylene flames at low pressure can be found in [4]. A comparable study on laminar *m*-xylene flames does not exist.

2. Experiment and theoretical calculations

A fuel-rich (Φ=1.79) *m*-xylene flame at 40 mbar with a cold gas velocity of 35 cm/s (at 300 K) with 50% argon dilution was studied at similar conditions as *o*-xylene in [4]. The measurements were performed with the MBMS setup at the Swiss Light Source. A detailed description of this system can be found in [19-21] and in the supplemental material. Procedures for the evaluation of species mole

fractions follow the procedure in [22] with modifications described in [19] and the supplemental material.

Species identification is achieved by comparison of measured ionization energies, PIE curves, and TPES with values of expected intermediates from the literature. For some species ionization energies were calculated using CBS-QB3 methods as implemented in Gaussian09 [23] suit of programs and photoelectron spectra were obtained by computing Franck-Condon factors with the program ezSpectrum.OSX [24]. Table S1 in the supplemental material gives a summary of the calculated ionization energies of possible intermediate species in the *m*-xylene flame.

3. Results

3.1 Mole fraction profiles and comparison to kinetic modeling results

The experimental mole fraction profiles of the major species and several combustion intermediates in the fuel-rich *m*-xylene flame are compared to modeling results using five current kinetic mechanisms from the literature [8, 10, 13, 25, 26]. The mechanism of Ranzi et al. [25] does not distinguish between the three xylene isomers but it includes a formation mechanism of PAHs up to C_{20}. The mechanism of Diévart et al. [26] for the combustion of 1,3,5-trimethylbenzene contains an oxidation sub-model for *m*-xylene assembled from the studies of [6] and [10]. Gudiyella [8] developed a model for the decomposition of *m*-xylene for high-pressure conditions based on their previous toluene and *m*-xylene oxidation model [27, 28] which also includes the formation and the decay of *p*-xylylene based on the work of [16]. The kinetic model of Mouis [13] is based on the toluene mechanism of Sivaramkrishnan et al. [29] and the *m*-xylene mechanism of Battin-Leclerc [6]. Finally, the mechanism of Gaïl and Dagaut [10] was developed from a previous reaction mechanism of the oxidation of *p*-xylene [9] and was also tested against low-pressure measurements. A rearrangement of the *m*-xylyl radical, which was observed in [14, 15] and will be discussed later, is not included in any of the models. In [8, 10, 26] the isomerization is implied by considering the direct formation of *p*-xylylene from the *m*-xylyl radical (*m*-$CH_3C_6H_4CH_2$ = *p*-$CH_2C_6H_4CH_2$ + H).

The one-dimensional temperature profile used in the kinetic modeling was calculated from the temperature dependence of the flow rate through the quartz sampling probe which is proportional to the pressure in the intermediate chamber. It was shown elsewhere [30] that this procedure is well-suited to obtain temperature profiles for kinetic modeling. The exhaust gas temperature was taken from [4] where a temperature profile was measured by a BeO-coated thermocouple for a *o*-xylene flame with same pressure, stoichiometry, and cold gas flow conditions as our flame. The one-dimensional flame simulations were carried out with the software library Cantera [31].

Figure 1 shows the experimental and simulated major species (Ar, O_2, *m*-C_8H_{10}, H_2, H_2O, CO, and CO_2) mole fraction profiles of the fuel-rich *m*-xylene flame investigated here. An enlarged figure can be found in the supplemental material (Fig. S3). In general, all five models reproduce the measured mole fractions well over the entire height above the burner (HAB). There are some discrepancies in the slope of the mole fraction profiles of H_2 and H_2O while the consumption of fuel and oxygen is captured well. Deviations in the exhaust gas concentration are within an acceptable error margin of 10%. Neither the experimental nor the simulated profiles were shifted for comparison.

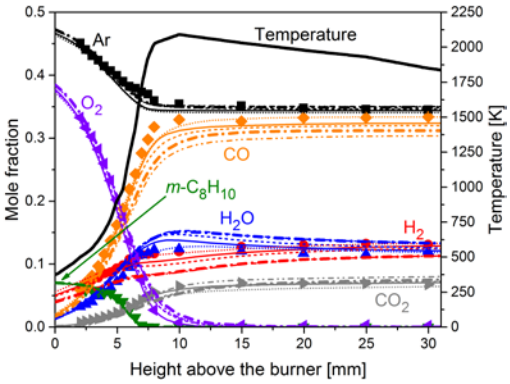

Figure 1. Experimental (symbols) major species mole fractions in comparison to simulations done with the models of Ranzi (solid line), Diévart (----), Gudiyella (····), Mouis (-···), Dagaut (-··-) and the flame temperature profile.

Overall, more than 30 combustion intermediates were identified and most of them were quantified. Table S2 in the supplemental material summarizes the information on literature and measured

ionization energies, calculated maximum mole fractions, and used cross section values for the quantitative evaluation of the intermediate species pool in the *m*-xylene flame. All mole fraction profiles and the temperature profile used for kinetic modeling are also provided in the supplemental material. When ionization energies for species with the same mass are too close for species separation the mole fraction was calculated with the photoionization cross section of the species expected to be dominant, e.g. for ketene and propene at *m/z*=42. Figure 2 shows some mole fraction profiles of measured intermediate species in the *m*-xylene flame in comparison to the kinetic modeling results. In general, all models can predict the peak positions well for a large number of combustion intermediates but there are also some differences between the experimental and simulated peak positions and between the models. Especially, the absolute concentration of the *m*-xylyl radical, the first decomposition intermediate species, is distinctly underestimated by all models.

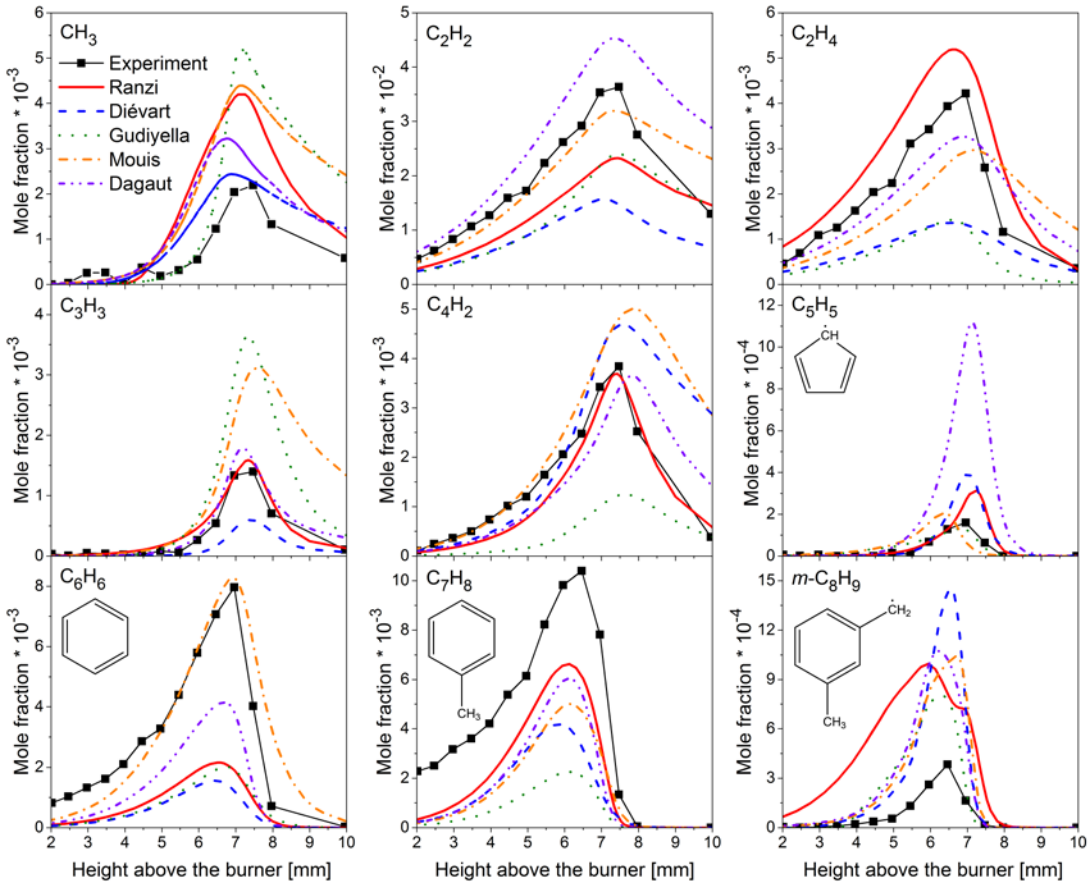

Figure 2. Experimental mole fraction profiles of some combustion intermediates in comparison to simulated mole fractions.

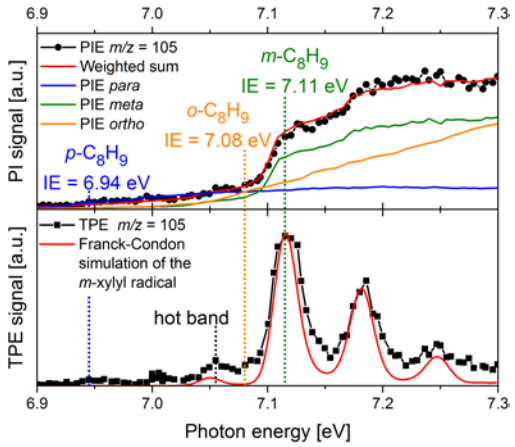

Figure 3. TPE spectrum and PIE curve of *m/z*=105 measured in the rich *m*-xylene flame compared to a Franck-Condon simulation of the *m*-xylyl radical and PIE curves of the xylyl radicals obtained from pyrolysis experiments.

3.2 Decomposition of *m*-xylene

For *m*-xylene we expect the *m*-xylyl radical (C_8H_9) as the dominant fuel radical. This radical can be clearly identified from the measured TPES in the reaction zone. Figure 3 shows the TPE signal of *m/z*=105, measured at HAB = 6.5 mm, in comparison to the Franck-Condon simulation from [15]. Ionization energies of the three xylyl isomers obtained from [15] are indicated. The sharp peak in our measured TPES fits perfectly to the adiabatic ionization energy of m-xylyl (7.11 eV) and also matches the calculated TPES very well. The two other characteristic peaks result from C-C-C bending and C-C stretching vibrations, respectively. The small peak at 7.06 eV is assigned to a hot-band transition, which was also observed in [15]. The presence of the other xylyl radicals (*o*-xylyl and *p*-xylyl radical), which have ionization energies of 7.08 and 6.94 eV [15], cannot be verified by the measured TPE spectrum. This observation would match initially the investigations of Li [3] where in fuel-rich xylene flames only the corresponding xylyl radicals were detected (i.e. only *m*-xylyl radical in *m*-xylene flames). However, there is a small peak in the ms-TPES below 7 eV, which might be a contribution of the *para* isomer present in very low concentration. A comparison of the PIE curves from the pyrolysis experiments [15] of all xylyl radicals to the PIE curve of *m/z*=105 obtained in the xylene flame shows that the ratio of *p*-xylyl to *m*-xylyl is approximately 15:85

indicating that small amounts of *p*-xylyl are present in the flame. The contribution of *o*-xylyl is negligible at this HAB. Direct hydrogen abstraction on the aromatic ring generating dimethylphenyl radicals (*m*-$CH_3C_6H_4CH_3$ = *m*-$CH_3C_6H_3CH_3$ + H) is less likely due to bond energy considerations. The formation of methylphenyl radicals by dissociation of the C-CH_3 bond (*m*-$CH3C_6H_4CH_3$ = $C_6H_4CH_3$ + CH_3), as proposed by da Silva et al., is more likely [32]. Of course, methylphenyl radicals can easily isomerize to the benzyl radicals which are the most stable C_7H_7 isomers and dominant intermediates formed during the combustion of alkylated aromatics [33]. Benzyl radicals were also identified here as the dominant C_7H_7 isomers by the strong fundamental transition in the ms-TPES at 7.25 eV (Fig. 4.), which agrees well with the literature ionization energy of 7.242 eV [34]. The onset at about 7 eV indicates that an additional C_7H_7 isomer must be present. The most stable isomers following benzyl are the tropyl and vinylcyclopentadienyl radicals [35]. Both can be excluded from consideration because their ionization energies are 6.23 [36] and 7.94 eV [37], respectively. The calculated ionization energies of the methylphenyl radicals are significantly higher (Table S1) and can also be excluded. However, calculated ionization energy of the 3-ethynylcyclopentenyl radical (7.04 eV) and the Franck Condon simulation fit the experimental spectrum well. Another route of benzyl radical formation proceeds via toluene which can be found in high amounts in the investigated flame (maximum mole fraction of 10^{-2}) and is underpredicted by a factor of two by the reaction models. In the iPEPICO setup coincident ion signal is lost if the kinetic energy release of the electrons exceeds 0.8 eV. This is the case here for toluene so that its mole fraction has a rather high uncertainty (see supplemental material). Toluene and benzyl are formed directly from the fuel (*m*-$CH_3C_6H_4CH_3$ + H = $C_6H_5CH_3$ + CH_3) by substitution of the methyl group by a hydrogen atom [10, 28], followed by a subsequent H-abstraction.

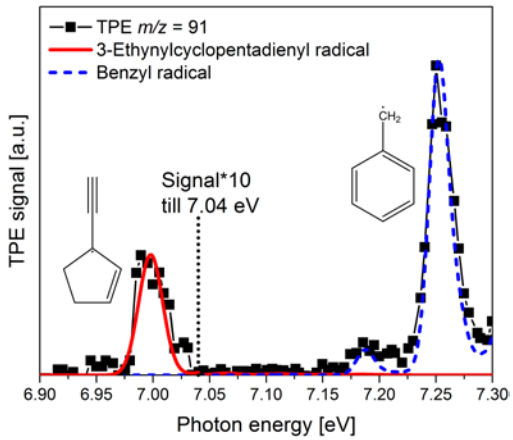

Figure 4. TPE spectrum of *m/z*=91 (symbols) in comparison to Franck-Condon simulations of 3-ethynylcyclopentadienyl radical (solid line) and benzyl radical (····).

On the other hand, decomposition of the *m*-xylyl radical leads to C_8H_8 species, which were identified by Franck-Condon simulations as *p*-xylylene, styrene, and benzocyclobutene (see Fig. 5). The PIE curve shows a first onset matching the adiabatic ionization energy of *p*-xylylene. So, the presence of *o*-xylylene, which has a lower ionization energy than *p*-xylylene, can be excluded at this position of the flame (6.5 mm). Similar observations were also made in a heated SiC reactor in previous work by Hemberger et al. [14, 15], where different reactor temperatures showed different C_8H_8 isomer compositions depending also on the prepared xylyl radical. The TPE spectrum of *m/z*=104 obtained from pyrolysis of *m*-xylyl bromide at 1300 K surface temperature is also shown in Fig. 5. Similar to the reaction zone of the laminar flame at 1100 K the same species pool was observed in the reactor, too.

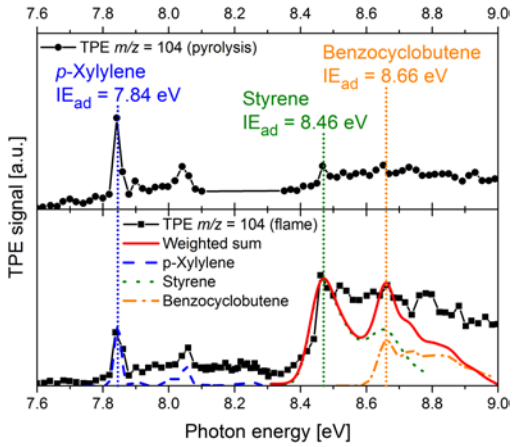

Figure 5. Measured TPE spectrum of m/z=104 (C_8H_8) in pyrolysis (top) and flame (bottom) experiments and comparison to Franck-Condon simulations of p-xylylene (----), styrene (····), and benzocyclobutene (-···,). The weighted sum of the Franck-Condon simulations is depicted as solid line.

m-Xylylene is in comparison to *o*- and *p*-xylylene a diradical and was not observed in our measurements or in [14-16] so that a rearrangement of the *m*-xylyl to the *p*-xylyl and the *o*-xylyl radical, respectively, must take place to obtain either *p*-xylylene [14] or styrene and benzocyclobutene. However, the *o*-xylyl radical was not found in the reaction zone of the fuel-rich flame (see Fig. 3). It was shown in [15] that the *o*-xylyl radical forms benzocyclobutene after H-bond scission via isomerization of *o*-xylylene. The presence of benzocyclobutene indicates that this reaction also occurs here, although the *o*-xylylene could not be detected. Benzocyclobutene itself isomerizes to styrene [14, 38] and was identified by the peak at 8.66 eV which matches the measured and calculated value of the adiabatic ionization energy of 8.65 eV [15]. Styrene can be found with the highest concentration of all C_8H_8 isomers (maximum mole fraction is twice as big as mole fraction of *p*-xylylene). The models of [10] and [13] predict the highest concentration for styrene and according to a reaction path analysis (see also Fig. S4) it is formed mainly by decomposition of Ethylbenzene. The decomposition steps of *m*-xylene to C_8H_8 isomers inferred from flame and reactor experiments lead to similar conclusions and are summarized in Fig. 6. Interestingly, the mole fraction of the fuel-radical is overestimated by all models compared to the measured concentration

profile and indicates that reactions for its degradation could be missing. However, it must be considered that the ionization cross section of the xylyl radical is unknown and had to be estimated to calculate the mole fraction (see supplemental material). Although *p*-xylyl and *o*-xylyl radicals were not unambiguously detected, their formation by rearrangement of the *m*-xylyl radical must take place. The reaction pathway to *p*-xylylene and benzocyclobutene in Fig. 6, including the isomerization of the xylyl radicals, is absent from all models. According to [4], benzocyclobutene will take part in the formation of indane and indene. Consequently, aromatics growths in this flame may be promoted by the reaction sequence and it should be included in the reaction mechanisms.

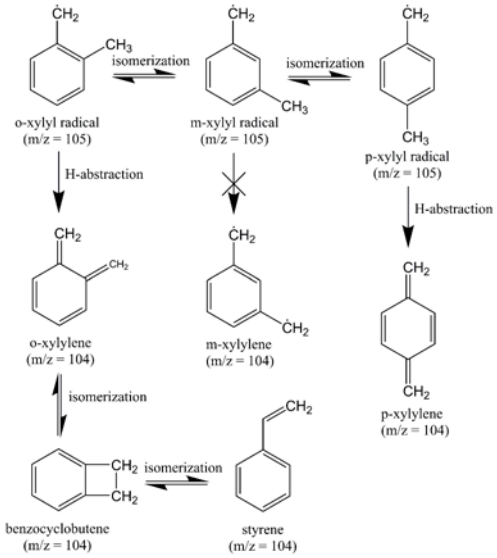

Figure 6. Decomposition steps of m-xylyl to C_8H_8 isomers.

Ring contraction to five-membered ring species starts by the decomposition of the *m*-xylyl radical yielding methylcyclopentadienyl (C_6H_7) and acetylene or 1,3-cyclopentadiene (C_5H_6) and propargyl [10]. 1,3-cyclopentadiene was clearly identified with maximum mole fraction of $2.1 \cdot 10^{-4}$. The high concentration of cyclopentadienyl radical can be explained by H-abstraction from 1,3-cyclopentadiene. Three methylcyclopentadiene isomers can be identified by Franck-Condon profiles to the ms-TPES of m/z = 80 (Fig. 7). The formation of methylcyclopentadiene as C_6H_8 isomer is highly probable because of the presence of the cyclopentadienyl radical while formation of the six-membered 1,3-cyclohexadiene from the fuel is less likely.

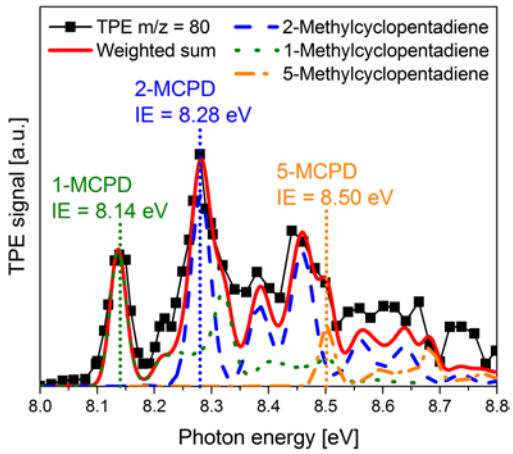

Figure 7. TPE spectrum of *m/z*=80 (symbols) in comparison to Franck-Condon simulations for 2-Methylcyclopentadiene (----), 1-Methylcyclopentadiene (⋯), and 5-Methylcyclopentadiene (-·-·).

3.3 Soot precursors and PAH formation

Because of the aromatic ring in *m*-xylene the sooting tendency and formation of PAHs is expected to be high under fuel-rich conditions. The formation of the first aromatic ring is often the kinetic bottleneck of higher PAH formation for aliphatic hydrocarbons. For *m*-xylene, as an aromatic hydrocarbon, the reaction path analysis (see Fig. S4) shows that benzene is mainly formed in the reaction zone from immediate fuel decomposition products like toluene ($C_7H_8 + H = C_6H_6 + CH_3$) and methylcyclopentadienyl radicals ($C_6H_7 = C_6H_6 + H$).

PAHs are included in the model of [25]. Reflecting the formation of substituted benzenes and benzene in few steps from the fuel in the reaction zone, naphthalene and indene are mainly formed by the reaction of methylphenyl radicals with propargyl. Mole fraction profiles of C_3H_3 and C_6H_6 are shown in Fig. 2. The general shape and the peak position are well predicted by all models but absolute mole fraction values differ. As discussed above, the methylphenyl radicals could not be observed experimentally here.

In aliphatic fuels benzene is often formed by recombination of propargyl radicals or the reactions of C_4H_3 or C_4H_5 with acetylene [39]. The reaction path analysis shows that these reactions are of minor importance for the formation of benzene here. However, in particular the C_4H_5 and C_4H_3 radicals are

formed during the oxidation of benzene under these fuel-rich conditions and the ability of a model to capture their mole fractions correctly may help to decide if the benzene oxidation pathways are implemented correctly.

In case of the C_4H_3 and C_4H_5 isomers, the resonantly stabilized *i*-isomer is more stable than the *n*-isomer [39] but we found only the *i*-isomer for C_4H_3 while for C_4H_5 the observed ionization energy of 7.94 eV fits to the calculated and evaluated ionization energies of 1-methylallenyl radical (CH_3CCCH_2) and 1-butyn-3-yl radical (CH_3CHCCH) from [39] or also to the 2-butyn-1-yl radical (CH_3CCCH_2) from [40]. All three species have similar ionization energies so that a distinction is not possible but *n*-C_4H_5 and *i*-C_4H_5 have lower ionization energies and can definitely be excluded. Also the model of [13], which includes the *n*-C_4H_5, *i*-C_4H_5 and 2-butyn-1-yl radicals, predicts the latter one with the highest mole fraction from decomposition of benzene (C_6H_6 + H = CH_3CCCH_2 + C_2H_2). Apart from benzene, fulvene is the second C_6H_6 isomer and its maximum mole fraction is about a factor of 100 smaller than for benzene. The maximum mole fraction of fulvene is 0.5 mm closer to the burner than the maximum of benzene (Table S2) which mirrors the fact that fulvene plays a role in benzene formation by direct or H-catalyzed isomerization [41].

Table S2 provides an overview of the experimentally clearly identified PAHs; PAHs for which assignment proved difficult are not reported. The mole fraction profiles of selected PAHs are shown in Fig. 8 and are compared to the simulation results obtained from the kinetic model of Ranzi [25]. Absolute mole fractions of the indenyl radical and naphthalene are well predicted while peak positions differ. The opposite is true for indene and the methylnaphthalenes indicating the need for further investigation.

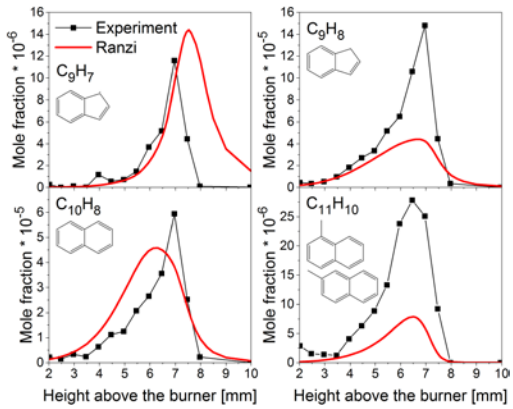

Figure 8. Mole fraction profiles of some PAHs compared to modeling results.

More PAHs up to *m/z*=200 were detected in an energy scan at 6.5 mm but the signal in the burner scans was too weak for quantification. Figure 9 shows a mass spectrum taken at 8.5 eV with mass gaps of 14 amu, presumably due to methyl addition followed by hydrogen abstraction. A sequence, starting with indene at *m/z*=116 followed by *m/z*=130 and 144 or starting from naphthalene (*m/z*=128) signals at *m/z*=142, 156, and 170 can be observed. The large number of possible isomers and the lack of measured ionization energies prevent identification, in particular for aromatics with more than two benzene rings.

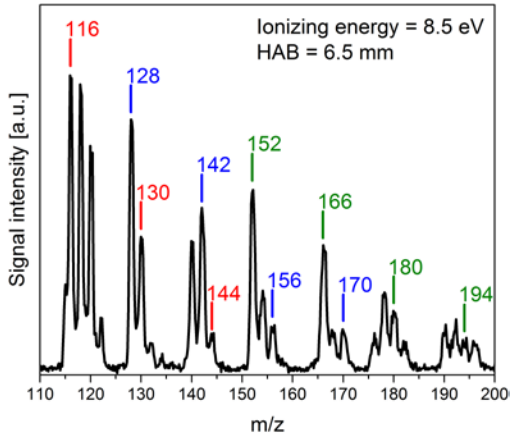

Figure 9. Mass spectrum of a series of PAHs with mass gap of 14 amu recorded in *m*-xylene.

4. Conclusions

In this study reactive intermediates were identified in a fuel-rich flame of *m*-xylene by imaging photoelectron photoionization coincidence spectroscopy at the SLS. The iPEPICO experiment allows

for simultaneous identification of combustion species with PIE and TPE spectra. TPE spectra give the fingerprint for each molecule so that unprecedented isomer resolution can be achieved. The new instrument at the SLS provides access to and reliable identification of previously unobserved species like *p*-xylylene or benzocyclobutene formed during combustion under low-pressure conditions. The mole fraction data were compared to simulations with current literature mechanisms. In general, the main species profiles, the maximum mole fraction for most combustion intermediates and the shape of the profiles can be reproduced quite well by all five kinetic models. For the initial steps of fuel destruction, agreement is less satisfactory. In particular, the experimental data presented here demonstrate a need to include the isomerization of *m*-xylyl to *o*- and *p*-xylyl radicals in updated combustion models. A few two-ring aromatic hydrocarbons can only be compared to one model and deviations caused by experimental uncertainties are mostly due to the lack of photoionization cross sections on the one hand and insufficient experimental data for model development on the other hand.

Xylyl radical pyrolysis experiments proved to be extremely useful in the analysis and interpretation of the flame data and show that these experiments, while not providing validation data for kinetic mechanism development directly, can contribute significantly to an understanding of flame chemistry.

Acknowledgments

The experiment was carried out at the VUV beamline at the Swiss Light Source of the Paul Scherrer Institute. T.B. and T.K. are grateful for financial support from the Ministry of Innovation, Science and Research of the German state of North Rhine-Westphalia. P.H. acknowledges funding by the Swiss Federal Office for Energy under BFE Contract No. 101969/152433 and SI/501269-01. Funding by the Helmholtz Association is acknowledged by P.O. and M.K. All authors acknowledge funding by the DFG under contract KA3871/3-1.

References

[1] International Energy Agency, World Energy Outlook, 2012.

[2] M. Figueroa, O. Lah, L.M. Fulton, A. McKinnon, G. Tiwari, Annual Review of Environment and Resources, 39 (2014) 295-325.

[3] Y.Y. Li, L.D. Zhang, T. Yuan, K.W. Zhang, J.Z. Yang, B. Yang, F. Qi, C.K. Law, Combust. Flame, 157 (2010) 143-154.

[4] L. Zhao, Z. Cheng, L. Ye, F. Zhang, L. Zhang, F. Qi, Y. Li, Proc. Combust. Inst., 35 (2015) 1745-1752.

[5] Y. Di, C.S. Cheung, Z. Huang, Atmospheric Environment, 43 (2009) 2721-2730.

[6] F. Battin-Leclerc, R. Bounaceur, N. Belmekki, P.A. Glaude, Int. J. Chem. Kinet., 38 (2006) 284-302.

[7] H.-P.S. Shen, M.A. Oehlschlaeger, Combust. Flame, 156 (2009) 1053-1062.

[8] S. Gudiyella, T. Malewicki, A. Comandini, K. Brezinsky, Combust. Flame, 158 (2011) 687-704.

[9] S. Gail, P. Dagaut, Combust. Flame, 141 (2005) 281-297.

[10] S. Gail, P. Dagaut, Combust. Sci. Technol., 179 (2007) 813-844.

[11] R.J. Johnston, J.T. Farrell, Proc. Combust. Inst., 30 (2005) 217-224.

[12] C.S. Ji, E. Dames, H. Wang, F.N. Egolfopoulos, Combust. Flame, 159 (2012) 1070-1081.

[13] A.G. Mouis, A. Menon, V. Katta, T.A. Litzinger, M. Linevsky, R.J. Santoro, S.P. Zeppieri, M.B. Colket, W.M. Roquemore, Combust. Flame, 159 (2012) 3168-3178.

[14] P. Hemberger, A.J. Trevitt, E. Ross, G. da Silva, J. Phys. Chem. Lett., 4 (2013) 2546-2550.

[15] P. Hemberger, A.J. Trevitt, T. Gerber, E. Ross, G. da Silva, J. Phys. Chem. A, 118 (2014) 3593-3604.

[16] G. da Silva, E.E. Moore, J.W. Bozzelli, J. Phys. Chem. A, 113 (2009) 10264-10278.

[17] E. Dames, H. Wang, Proc. Combust. Inst., 34 (2013) 307-314.

[18] C.S. McEnally, L.D. Pfefferle, Combust. Flame, 148 (2007) 210-222.

[19] P. Oßwald, P. Hemberger, T. Bierkandt, E. Akyildiz, M. Kohler, A. Bodi, T. Gerber, T. Kasper, Rev. Sci. Instrum., 85 (2014) 11.

[20] A. Bodi, M. Johnson, T. Gerber, Z. Gengeliczki, B. Sztaray, T. Baer, Rev. Sci. Instrum., 80 (2009) 7.

[21] A. Bodi, P. Hemberger, T. Gerber, B. Sztaray, Rev. Sci. Instrum., 83 (2012) 8.

[22] T.A. Cool, A. McIlroy, F. Qi, P.R. Westmoreland, L. Poisson, D.S. Peterka, M. Ahmed, Rev. Sci. Instrum., 76 (2005) 7.

[23] M.J. Frisch, G.W. Trucks, H.B. Schlegel, G.E. Scuseria, M.A. Robb, J.R. Cheeseman, G. Scalmani, V. Barone, B. Mennucci, G.A. Petersson, H. Nakatsuji, M. Caricato, X. Li, H.P. Hratchian, A.F. Izmaylov, J. Bloino, G. Zheng, J.L. Sonnenberg, M. Hada, M. Ehara, K. Toyota, R. Fukuda, J. Hasegawa, M. Ishida, T. Nakajima, Y. Honda, O. Kitao, H. Nakai, T. Vreven, J.A. Montgomery, Jr., J.E. Peralta, F. Ogliaro, M. Bearpark, J.J. Heyd, E. Brothers, K.N. Kudin, V.N. Staroverov, R. Kobayashi, J. Normand, K. Raghavachari, A. Rendell, J.C. Burant, S.S. Iyengar, J. Tomasi, M. Cossi, N. Rega, J.M. Millam, M. Klene, J.E. Knox, J.B. Cross, V. Bakken, C. Adamo, J. Jaramillo, R. Gomperts, R.E. Stratmann, O. Yazyev, A.J. Austin, R. Cammi, C. Pomelli, J.W. Ochterski, R.L. Martin, K. Morokuma, V.G. Zakrzewski, G.A. Voth, P. Salvador, J.J. Dannenberg, S. Dapprich, A.D. Daniels, Ö. Farkas, J.B. Foresman, J.V. Ortiz, J. Cioslowski, D.J. Fox, Gaussian 09, Revision C.01, Gaussian, Inc., Wallingford CT, 2009.

[24] V.A. Mozhayskiy, A.I. Krylov, ezSpectrum, http://iopenshell.usc.edu/downloads.

[25] E. Ranzi, A. Frassoldati, R. Grana, A. Cuoci, T. Faravelli, A.P. Kelley, C.K. Law, Prog. Energy Combust. Sci., 38 (2012) 468-501.

[26] P. Dievart, H.H. Kim, S.H. Won, Y.G. Ju, F.L. Dryer, S. Dooley, W.J. Wang, M.A. Oehlschlaeger, Fuel, 109 (2013) 125-136.

[27] R. Sivaramakrishnan, R.S. Tranter, K. Brezinsky, Combust. Flame, 139 (2004) 340-350.

[28] J.L. Emdee, K. Brezinsky, I. Glassman, J. Phys. Chem., 95 (1991) 1626-1635.

[29] R. Sivaramakrishnan, R.S. Tranter, K. Brezinsky, Proc. Combust. Inst., 30 (2005) 1165-1173.

[30] M. Schenk, L. Leon, K. Moshammer, P. Osswald, T. Zeuch, L. Seidel, F. Mauss, K. Kohse-Hoinghaus, Combust. Flame, 160 (2013) 487-503.

[31] D.G. Goodwin, H.K. Moffat, R.L. Speth, Cantera: An Object-oriented Software Toolkit for Chemical Kinetics, Thermodynmics, and Transport Processes, http://www.cantera.org, Version 1.8, 2011.

[32] G. da Silva, C.C. Chen, J.W. Bozzelli, J. Phys. Chem. A, 111 (2007) 8663-8676.

[33] G. da Silva, J.W. Bozzelli, J. Phys. Chem. A, 113 (2009) 8971-8978.

[34] P.J. Linstrom, W.G. Mallard, Eds., NIST Chemistry WebBook, NIST Standard Reference Database Number 69, National Institute of Standards and Technology, Gaithersburg MD, http://webbook.nist.gov, (retrieved 2015).

[35] G. da Silva, J.A. Cole, J.W. Bozzelli, J. Phys. Chem. A, 114 (2010) 2275-2283.

[36] K.H. Fischer, P. Hemberger, A. Bodi, I. Fischer, Beilstein Journal of Organic Chemistry, 9 (2013) 681-688.

[37] J.D. Savee, T.M. Selby, O. Welz, C.A. Taatjes, D.L. Osborn, J. Phys. Chem. Lett., 6 (2015) 4153-4158.

[38] O.L. Chapman, U.P.E. Tsou, J.W. Johnson, J. Am. Chem. Soc., 109 (1987) 553-559.

[39] N. Hansen, S.J. Klippenstein, C.A. Taatjes, J.A. Miller, J. Wang, T.A. Cool, B. Yang, R. Yang, L.X. Wei, C.Q. Huang, J. Wang, F. Qi, M.E. Law, P.R. Westmoreland, J. Phys. Chem. A, 110 (2006) 3670-3678.

[40] M. Lang, F. Holzmeier, P. Hemberger, I. Fischer, J. Phys. Chem. A, 119 (2015) 3995-4000.

[41] A.W. Jasper, N. Hansen, Proc. Combust. Inst., 34 (2013) 279-287.

List of supplemental material:

Word document includes Table S1, Table S2, Figure S3, Figure S4 and additional information about the experiment, the data reduction and species identification.

Excel sheet includes the temperature profile used for kinetic modeling and the calculated mole fraction profiles of the observed species.

List of figure captions:

Figure 1. Experimental (symbols) major species mole fractions in comparison to simulations done with the models of Ranzi (solid line), Diévart (----), Gudiyella (····), Mouis (-···), Dagaut (-···) and the flame temperature profile.

Figure 2. Experimental mole fraction profiles of some combustion intermediates in comparison to simulated mole fractions.

Figure 3. TPE spectrum and PIE curve of *m/z*=105 measured in the rich *m*-xylene flame compared to a Franck-Condon simulation of the *m*-xylyl radical and PIE curves of the xylyl radicals obtained from pyrolysis experiments.

Figure 4. TPE spectrum of *m/z*=91 (symbols) in comparison to Franck-Condon simulations of 3-ethynylcyclopentadienyl radical (solid line) and benzyl radical (····).

Figure 5. Measured TPE spectrum of m/z=104 (C_8H_8) in pyrolysis (top) and flame (bottom) experiments and comparison to Franck-Condon simulations of p-xylylene (----), styrene (····), and benzocyclobutene (-···,). The weighted sum of the Franck-Condon simulations is depicted as solid line.

Figure 6. Decomposition steps of m-xylyl to C_8H_8 isomers.

Figure 7. TPE spectrum of *m/z*=80 (symbols) in comparison to Franck-Condon simulations for 2-Methylcyclopentadiene (----), 1-Methylcyclopentadiene (····), and 5-Methylcyclopentadiene (-···).

Figure 8. Mole fraction profiles of some PAHs compared to modeling results.

Figure 9. Mass spectrum of a series of PAHs with mass gap of 14 amu recorded in *m*-xylene.